Acknowledgments

The authors express their gratitude to Engineering and Physical Sciences Research Council (EPSRC) and Defence Evaluation and Research Agency (DERA) Bedford for their financial support during this work. We also thank J. H. Whitelaw and P. Bearman for their advice and support.

References

[1]Gionet, C., and Yandrasts, F., "Developments in Model Design and Manufacturing Techniques," Royal Aeronautical Society 1997 European Forum, Wind Tunnels and Wind Tunnel Test Techniques, April 1997.

[2]Springer, A., Cooper, K., and Roberts, F., "Application of Rapid Prototyping Models to Transonic Wind Tunnel Testing," AIAA Paper 97-0988, 1997.

[3]Springer, A., and Cooper, K., "Comparing the Aerodynamic Characteristics of Wind Tunnel Models Produced by Rapid Prototyping and Conventional Methods," AIAA Paper 97-2222, 1997.

[4]Landrum, D. B., Beard, R. M., Lasarge, P. A., and von Sprecken, N., "Evaluation of Stereolithography Rapid Prototyping for Low Speed Airfoil Desing," AIAA Paper 97-0719, 1997.

[5]Chuk, R. N., and Thomson, V. J., "Comparison of Rapid Prototyping Techniques Used for Wind Tunnel Model Fabrication," *Rapid Prototyping Journal*, Vol. 4, No. 4, 1998, pp. 185–196.

Aerodynamic Characteristics of Deflected Surfaces in Compressible Flows

Kung-Ming Chung*
National Cheng Kung University, Tainan 711, Taiwan, Republic of China

Nomenclature

C_p	=	pressure coefficient, $(p_w - p_\infty)/q_\infty$
M	=	freestram Mach number
p_w	=	surface static pressure
q_∞	=	dynamic pressure
x	=	coordinate along the surface of the corner
x^*	=	x/δ_0
x_d^*	=	downstream influence region, x_d/δ_0
x_u^*	=	upstream influence region, x_u/δ_0
Δc_D	=	lift-induced-drag coefficient
Δc_L	=	incremental lift coefficient
δ_0	=	incoming boundary-layer thickness
η	=	deflected angle

Introduction

THE flap can be used as the high-lift device, in which a deflection downward results in the gain in lift at the given geometric angle of attack. For the influence of small flap deflections, a straight line from the leading to trailing edges of a symmetrical airfoil at zero angle of attack is treated as the fictitious chord line. The problem is reduced to a camber airfoil at an angle of attack. The incremental lift coefficient and moment coefficient about the aerodynamic center vary with the flap deflection and can be predicted by thin-airfoil theory. The magnitudes are related to the distance of the hinge line behind the leading edge.[1] Note that the agreement between theory and experiment is poor due to the boundary-layer effect. Furthermore, Bolonki and Gilyard[2] indicated that the deflected control surfaces could be used in combination to provide variable camber control within the operational flight envelope of a civil aircraft. At cruise speeds, the benefits of variable camber using a simple trailing-edge control surface system could approach more than 10% in maximizing the lift-to-drag ratio, especially for nonstandard flight conditions. However, the critical Mach number, onset of boundary-layer separation, and drag are also strongly related to the allowable deflection of the control surfaces.

A simplified model of a deflected surface was studied by Chung.[3–5] On the upper deflected surface (or convex-corner flow), strong upstream expansion and downstream compression are observed near the corner in compressible flows. The interaction region can be scaled with the freestream Mach number and the convex-corner angle, $M^2\eta$. The boundary layer downstream of the corner is separated at $M^2\eta \geq 8.95$. The separation position moves slightly upstream and the reattachment position moves downstream with increasing convex-corner angle. On the lower deflected surface (or concave-corner flow), the flow decelerates upstream of the corner, followed by the downstream acceleration. The characteristics of the flow, for example, upstream compression, downstream expansion, and interaction region, are associated with the freestream Mach number and the concave-corner angle, $M\eta$.

To characterize the aerodynamic performance of a deflected surface in compressible flows, the present study reexamined a turbulent boundary layer past the convex and concave corners at $M = 0.64$ and 0.83 (Fig. 1). This investigation involved the analysis of mean surface pressure distributions of the convex- and concave-corner flows. The incremental lift and lift-induced-drag coefficients are estimated based on the characteristics or the integration of surface pressure distributions.

Experiment

Transonic Wind Tunnel

The Aerospace Science and Technology Research Center, National Cheng Kung University transonic wind tunnel is a blowdown type.[6] Major components of the facility include compressors, air dryers, cooling water system, storage tanks, and the tunnel. The dew point of high-pressure air through the dryers is maintained at -40°C under normal operation conditions. Air storage volume for the three storage tanks is up to 180 m^3 at 5.15 MPa. The test section is 600 mm square and 1500 mm long. In the present study, the test section was assembled with solid sidewalls and perforated top/bottom walls to reduce the background acoustic noise. The freestream Mach numbers were 0.64 and 0.83 ± 0.01, and the stagnation pressure p_0 and temperature T_0 were 172 ± 0.5 kPa and room temperature, respectively.

For the data acquisition system, the NEFF Instruments System 620 and the LeCroy waveform recorders were used. The test conditions were recorded by the NEFF system, whereas the LeCroy 6810 waveform recorders were used for the pressure measurements. A host computer with CATALYST software controlled the setup of LeCroy waveform recorders through a LeCroy 8901A interface. All input channels were triggered simultaneously by using an input channel as the trigger source.

Test Model

The test model consists of a flat plate and an interchangeable instrumentation plate. The test model is 150 mm wide and 600 mm long, which is supported by a single sting mounted on the

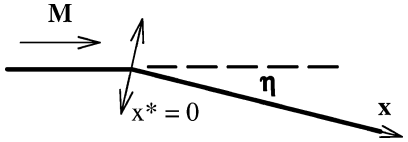

Fig. 1 Test configuration.

Received 9 October 2003; revision received 17 November 2003; accepted for publication 18 November 2003.

*Research Fellow, Aerospace Science and Technology Research Center, 2500 Section 1, Chung-Cheng South Road, Kueijen; kmchung@astrc.iaalab.ncku.edu.tw. Senior Member AIAA.

bottom wall of the test section. The concave corner with 3-, 5-, 7-, 10-, and 15-deg angles or the convex corner with 5-, 10-, 13-, and 15-deg angles is located at 500 mm from the leading edge of the flat plate. One row of 19 holes, 6 mm apart and 2.5 mm in diameter, was installed along the centerline of each instrumentation plate perpendicular to the test surface. All of the pressure transducers within the holes were flush mounted to the test surface and potted using silicone sealant. The side fences of the instrumentation plate were installed to prevent crossflow.

Experimental Techniques

For the surface pressure measurements, Kulite (Model XCS-093-25A, B screen) pressure transducers powered by a TES Model 6102 power supply at 15.0 V were used. The outside diameter is 2.36 mm, and the sensing element is 0.97 mm in diameter. External amplifiers (Ecreon Model E713) were used to improve the signal-to-noise ratio. The typical sampling period is 5 μs (200 kHz). Each data record possesses 131,072 data points for the statistical analysis. The data were divided into 32 blocks. The mean values of each block (4096 data points) were calculated. Variations of the blocks are estimated to be 0.43% for the mean surface pressure coefficient C_p, which is considered to be the uncertainty of experimental data.

For the characteristics of the incoming boundary layer, pitot pressure surveys were conducted at 25 mm upstream of the corner without the corner in place. The normalized velocity profiles appear to be full; $n \approx 7$–11 for the velocity power law. A study by Miau et al.[7] further indicated that the transition of the boundary layer under the present test condition is close to the leading edge of the flat plate. This indicates turbulent flow at the measurement locations. The boundary-layer thickness was estimated to be 7.3 and 7.1 ± 0.2 mm for $M = 0.64$ and 0.83, respectively.

Results and Discussion

Characteristics of Pressure Distribution

Examples of the mean surface pressure coefficients C_p along the centerline of the instrumentation plates are shown in Fig. 2. The solid symbol represents the mean surface pressure distributions on the upper surface of a deflected surface (or convex corner), whereas the filled symbol is for the lower surface (or concave corner). It can be seen that the flows accelerate upstream of the convex corner followed by the compression. Stronger upstream expansion and downstream recompression are associated with increasing convex-corner angle, and the minimum pressure is observed near the corner. Nearly constant pressure gradients (upstream expansion and downstream compression) are observed at subsonic speeds. For the transonic unseparated expansion flows ($M^2\eta \geq 6.14$), there are more intense pressure variations near the corner. Mild initial compression and larger interaction region are associated with the separated transonic expansion flows, $M = 0.83$ at $\eta = 10$ and 15 deg (Fig. 2b). On the lower surface, the pressure distributions of the concave-corner flow show similar in shape for all of the test cases. The flows decelerate upstream of the concave corner followed by the expansion. The interaction region tends to expand in both the upstream and downstream directions with larger concave-corner angle. Linear variations of upstream compression and downstream expansion are observed.

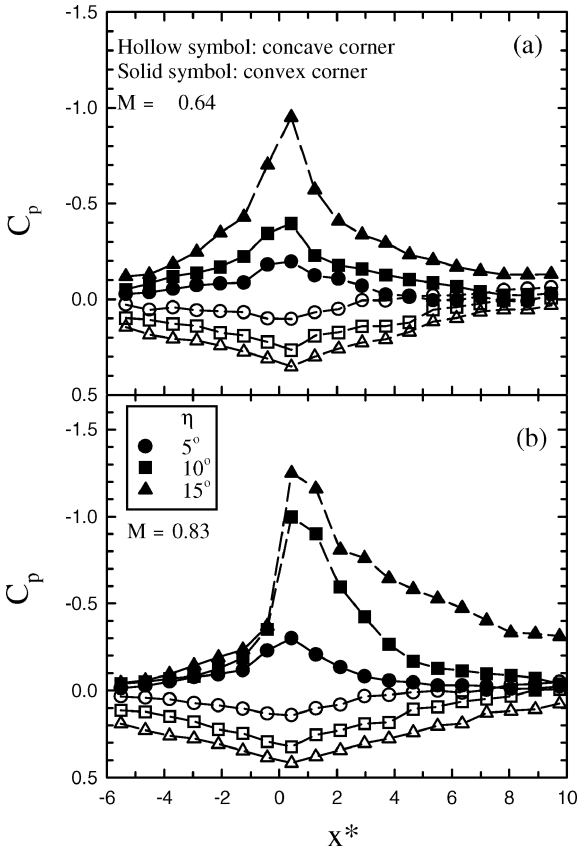

Fig. 2 Surface pressure distributions.

To obtain a quick estimation of the incremental aerodynamic coefficients of a deflected surface near the corner, the present study reexamines the characteristics of the mean surface pressure distributions. These include the upstream and downstream influence regions, the peak pressure near the corner, and the downstream pressure. The upstream influence x_u^* can be determined as the intercept of the tangent to the maximum pressure gradient with the undisturbed surface pressure (or $C_p = 0$).[8] The downstream influence x_d^* represents the distance for a disturbed boundary layer back to equilibrium status and can be estimated from the peak pressure near the corner to the intersection of the tangent through the downstream pressure data with the approximately equilibrium downstream pressure. Because adequate equilibrium downstream pressure can only be approximately obtained, the estimation of the downstream influence region is subject to more uncertainty. In Fig. 3, the interaction length for attached flows is scaled with $M^2\eta$ for the convex-corner flows and with $M\eta$ for the concave-corner flows. It can be seen that the upstream influence and downstream influence regions appear to increase linearly with $M^2\eta$ or $M\eta$. The extent of upstream influence region on the lower surface is considerably greater than that on the upper surface. The difference of downstream influence region is less significant.

The peak pressure $C_{p,\text{peak}}$ near the corner and the downstream surface pressure $C_{p,d}$ are also required to estimate the aerodynamic characteristics of a deflected surface. Figure 4 shows that these characteristic pressures can be scaled with $M^2\eta$ or $M\eta$ for the convex-corner or the concave-corner flows, respectively. The peak pressure and downstream surface pressure of the convex-corner flows are substantially decreased with increasing $M^2\eta$. The concave-corner flows show the opposite trend with $M\eta$, in which there is mild

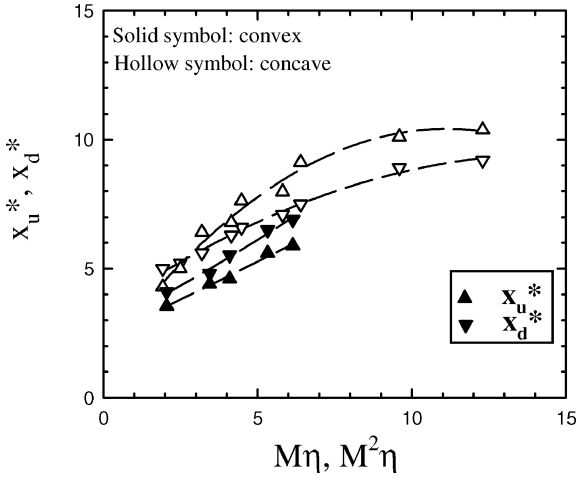

Fig. 3 Upstream/downstream influence.

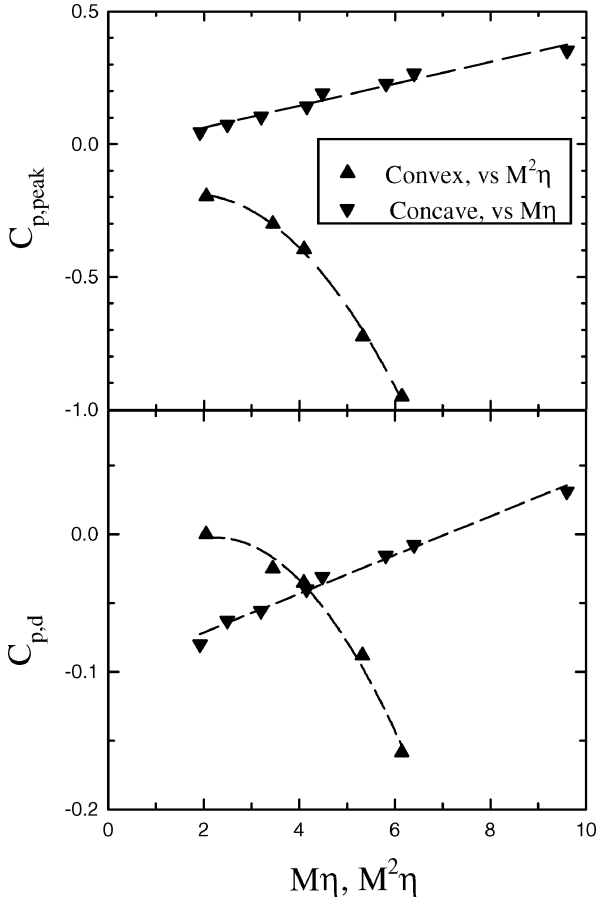

Fig. 4 Characteristic pressures.

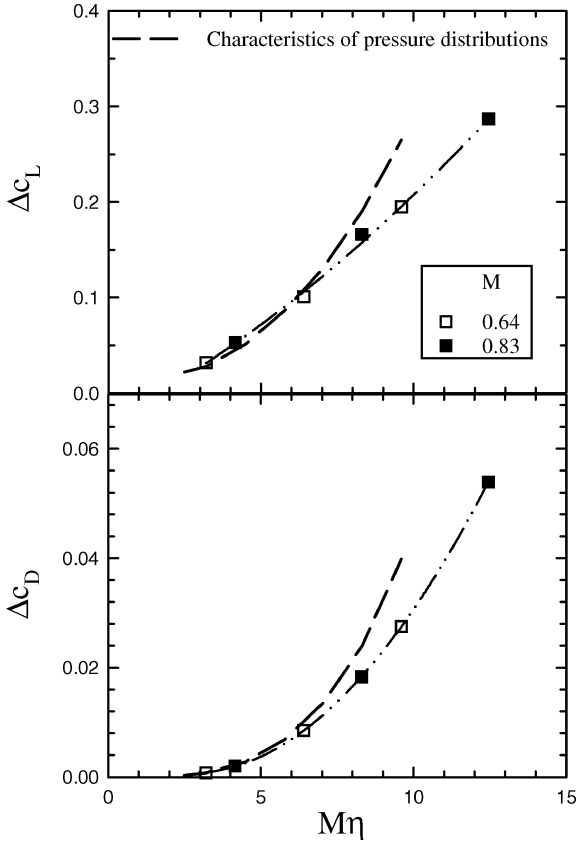

Fig. 5 Incremental lift and drag estimated by the integration of surface pressure.

variation of the pressure levels. The increasing expansion for the convex-corner flows (upper surface) and stronger compression for the concave-corner flows (lower surface) imply the increment of the lift coefficient with $M^2\eta$ or $M\eta$.

Aerodynamic Characteristics

Kuethe and Chow[1] indicated that the incremental lift coefficient varies linearly with the flap deflection for the incompressible flows. For the present study, the incremental lift and drag coefficients of the deflected surface can be simply estimated by the interaction regions and characteristic pressures for the attached flows. The variations of the incremental lift coefficient Δc_L and the lift-induced-drag coefficient Δc_D are shown in Fig. 5. It can be seen that Δc_L is up to 0.25 and appears to be a quadratic function of $M\eta$. The additional positive lift force also produces additional induced drag Δc_D, particularly at higher $M\eta$. The benefit with a simple deflected surface will, thus, decrease.

Furthermore, Δc_L and Δc_D ($M = 0.64$ and 0.83 at $\eta = 5$, 10, and 15 deg) are estimated by the integration of pressure distributions on the upper and lower surfaces. Figure 5a shows that Δc_L increases linearly with the deflection angle at $M = 0.64$ or 0.83. At a given deflection angle, higher Δc_L is also observed at $M = 0.83$ than that at $M = 0.64$. This corresponds to the compressibility effect. It is also observed that variation of Δc_L with $M\eta$ coincides reasonably well for both testing Mach numbers. Estimation of Δc_D is shown in Fig. 5b. For the attached flows on the upper surface (convex-corner flows at $M\eta \leq 9.6$), Δc_D increases gradually with $M\eta$. Substantial increase in Δc_D is observed with the separated flow on the upper surface at $M\eta = 12.45$ (or $M^2\eta = 10.33$). Furthermore, it can be seen that there is some disagreement with the aerodynamic coefficients estimated by the characteristics and the integration of the surface pressure distributions at $M\eta = 9.6$ (or $M^2\eta = 6.14$). On the upper surface (convex-corner flow), this corresponds to the transition of subsonic and transonic expansion flows.[4] Steeper upstream expansion and downstream compression result in the overestimation of the aerodynamic coefficients.

Conclusions

A simplified model of a deflected surface was studied. At subsonic speeds, the incremental lift coefficient and lift-induced-drag coefficient can be estimated from the interaction region and the characteristic pressures reasonably well. The effects of increasing deflection angle and freestream Mach number are observed, and the increment varies with the similarity parameter $M\eta$. Substantial increase in the lift-induced-drag coefficient is associated with the transonic separated flow on the upper surface.

Acknowledgments

The research was support by the National Science Council (NSC 90-2212-E-006-132). The support is gratefully acknowledged. The author also thanks the Aerospace Science and Technology Research Center, National Cheng Kung University technical staffs for technical support with the experiments.

References

[1]Kuethe, A. M., and Chow, C., *Foundations of Aerodynamics*, 3rd ed., Wiley, New York, 1976, pp. 133–138.

[2]Bolonki, A., and Gilyard, G. B., "Estimated Benefits of Variable-Geometry Wing Camber Control for Transport Aircraft," NASA TM-1999-206586, Oct. 1999.

[3]Chung, K., "Transition of Subsonic and Transonic Expansion Flows," *Journal of Aircraft*, Vol. 37, No. 6, 2000, pp. 1079–1082.

[4]Chung, K., "Investigation on Transonic Convex-Corner Flows," *Journal of Aircraft*, Vol. 39, No. 6, 2002, pp. 1014–1018.

[5]Chung, K., "An Experimental Study of Compressible Concave Corner Flows," 2002 International Conf. on the Methods of Aerophysics Research,

Inst. of Theoretical and Applied Mechanics, Russian Academy of Sciences, Siberian Branch, Novosibirsk, Russia, July 2002.

[6]Chung, K., "Development and Calibration of ASTRC/NCKU 600 × 600 mm Transonic Wind Tunnel," National Science Council, Rept. NSC 83-2212-E-006-141T, Taiwan, Republic of China, Aug. 1994.

[7]Miau, J., Cheng, J., Chung, K., and Chou, J., "The Effect of Surface Roughness on the Boundary Layer Transition," *Proceedings of the 7th International Symposium on Flow Modeling and Turbulence Measurements*, Tainan Taiwan, ROC, National Cheng Kung Univ., Oct. 1998, pp. 609–616.

[8]Lu, F. K., "Fin Generated Shock-Wave Boundary Layer Interactions," Ph.D. Dissertation, Dept. of Mechanical Engineering, Pennsylvania State Univ., University Park, PA, May 1988.

Estimation of Flight Load History Using Global Positioning System Data

Fredrik de Try*
Royal Institute of Technology, SE-100 44 Stockholm, Sweden

Introduction

THE Swedish jet trainer Saab 105 with Swedish Air Force designation SK60 has been in military service since the late 1960s and is today used for military pilot training. The need for monitoring the aircraft structural condition increases with increasing flight hours. Consequently, to instrument an old aircraft such as the SK60 with flight load recording devices can be expensive and invoke complicated procedures including new airworthiness tests. Here a cost effective method is used to estimate the flight load history of the aircraft using a global positioning system (GPS) receiver only.

The aircraft fatigue environment is mainly dependent on the normal accelerations of the aircraft, and hence, the load factor n_z is a suitable parameter for modeling this kind of problem. To obtain an overall view of the aircraft fatigue life, a load factor history can be performed counting the number of occurrences a certain load factor level is reached or exceeded for a given time interval. A large number of flights containing aircraft load factor data recorded by an accelerometer is normally divided into different flight missions or segments such as ascent, cruise, loiter, descent, etc. A load factor history is then calculated for the different segments to obtain the total number of load factor occurrences.[1] With use of this load factor history, the fatigue load environment of the aircraft can be predicted, but this part is excluded in this study.

The different SK60 used in the daily training are randomly distributed to the pilots before flight. Because the individual aircraft are changed from flight to flight, the pilots do not get used to the different aircraft characteristics and behavior. This also means that the different individual aircraft are exposed to similar loads over long time ranges.

The approach in this study is to use a fully instrumented reference SK60 measuring normal accelerations of the aircraft's center of gravity, which is directly related to the load factor n_z. To get an overall view of the load factor history of all of the other SK60 in the training squadron, it is proposed to instrument all of them with a GPS receiver and to use the reference aircraft for complementary information. The reference aircraft used in this study is the fully instrumented SK60:072 located at the Swedish Defence Materiel Administration (FMV) in Linköping, Sweden.

Received 14 October 2003; revision received 13 November 2003; accepted for publication 18 November 2003.

*Ph.D. Student, Department of Aeronautical and Vehicle Engineering. Member AIAA.

Load Factor History

Measuring the normal acceleration of the aircraft's center of gravity leads to the load factor n_z, which is given in units of gravitational acceleration, where $g = 9.81$ m/s^2, and the steady-state load factor is $n_z = 1.0\ g$. Load factor history tables or plots are usually separated into load factors greater than 1.0 g and load factors less than 1.0 g. A load factor exceedance is obtained if a certain load factor level is met or exceeded, that is, $n_z + \Delta n_z$, or $n_z - \Delta n_z$ during the time the load factor departs from the reference level 1.0 g to the time the load factor returns to 1.0 g. During this time, the load factor exceedance for a specific load factor level is only counted once and then is called an occurrence. Furthermore, a FORTRAN program has been developed in this study to perform the load factor occurrence calculations.

The load factor is often separated into two parts, maneuver load factors and load factors due to gusts. The maneuver load factors are typically of a lower frequency than the load factors caused by gusts. The load factors due to gusts are often estimated using a power spectral density method using an empirical model of the atmospheric turbulence together with the dynamics of the aircraft.[2]

Reference Aircraft

The operational SK60 of the Swedish Air Force are not equipped with any aircraft flight data recording system at all. The SK60:072 is stationed at FMV in Linköping and is specially instrumented with various devices for data recording during flight. The SK60:072 is equipped with an inertial measurement unit (IMU) that measures the accelerations and angular rates of the aircraft. The GPS receiver in the SK60:072 can provide positioning data at a frequency of 2 Hz. The IMU can provide the acceleration in the aircraft body normal direction at a frequency of 60 Hz. The GPS positioning data and the normal acceleration data from the IMU are used as reference data in this work. The number of flights made available for this study is strictly limited. Normal acceleration and GPS data for nine flights are used, but only three of them contain 2-Hz GPS data. The remaining six flights contain 1-Hz GPS data, which is too poor to model the maneuver load factors accurately, but the IMU data are still used from these flights.

Calculating the Maneuver Load Factors from GPS Data

A GPS receiver is a very powerful and widely used device for position and velocity determination of an aircraft.[3] In this study, the 2-Hz GPS positioning and velocity data are used to estimate the flight path in terms of a B-spline curve following the GPS records. In a previous study, a method involving a constrained least-squares approach to find a B-spline curve representing a smooth flight path suitable for flight visualization is successfully performed.[4] Because this method of estimating the load factor history needs to be performed for all of the flights, a fast method is desirable. Consequently, a less computationally intense interpolation approach is adopted here.

When a suitable knot vector is chosen, the linear system of equations for solving the B-spline coefficients can be formulated for the GPS velocity V_{GPS} as

$$\sum_{j=1}^{n} a_j N_{j,k}(t_i) = V_{\mathrm{GPS}}(t_i), \qquad i = 1, 2, \ldots, n \tag{1}$$

where n is the number of GPS velocity records and the $N_{j,k}(t_i)$ are the basis functions of order $k = 4$ calculated at the time instants t_i. The n unknown coefficients a_j are obtained by solving Eq. (1) using FORTRAN subroutines where the sparse banded structure is taken into account.[5] Similar calculations are performed to obtain smooth curves to represent the flight path angle γ_{GPS}, heading ψ_{GPS} and altitude h_{GPS}.

One advantage of using a curve fit to the GPS data for modeling the flight path is that the first derivative with respect to time can easily be calculated for any desired time instant of the flight path. Consequently, the flight path is estimated independently of an aircraft model.